atmosphere

MDPI

Supplementary Material

Analysis of Pollutant Dispersion in a Realistic Urban Street Canyon using Coupled CFD and Chemical Reaction Modeling

Franchesca G. Gonzalez Olivardia*, Qi Zhang, Tomohito Matsuo, Hikari Shimadera and Akira Kondo

Graduate School of Engineering, Osaka University, 2-1 Yamadaoka, Suita, Osaka 565-0871, Japan

* Correspondence: franchesca@ea.see.eng.osaka-u.ac.jp; Tel.: +81-6-6879-7668

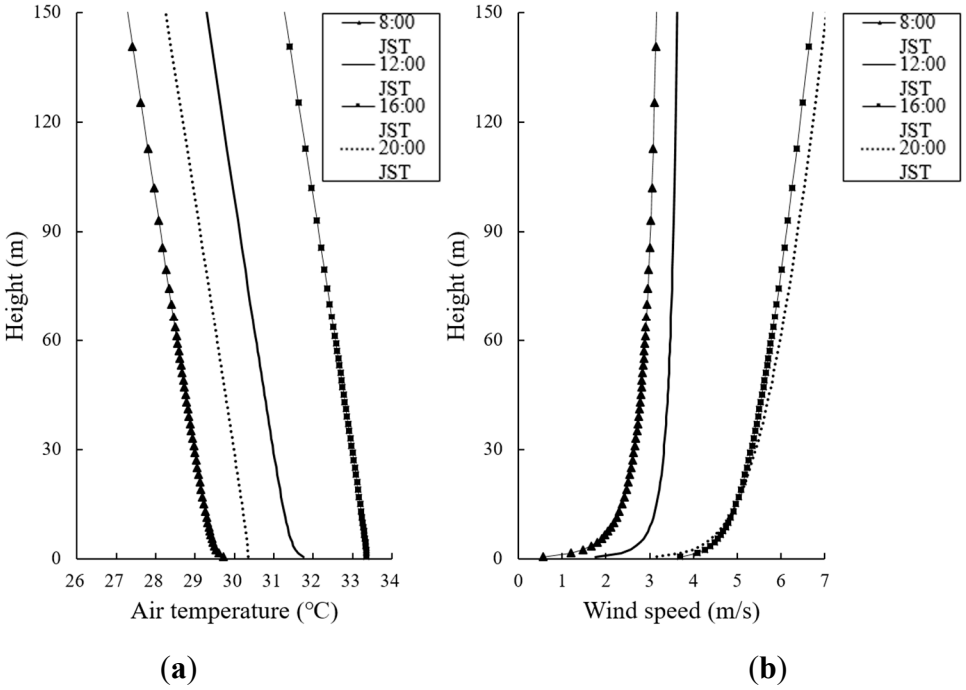

Figure S1. Boundary conditions for (**a**) air temperature and (**b**) wind speed at 08:00, 12:00, 16:00, and 20:00 JST.

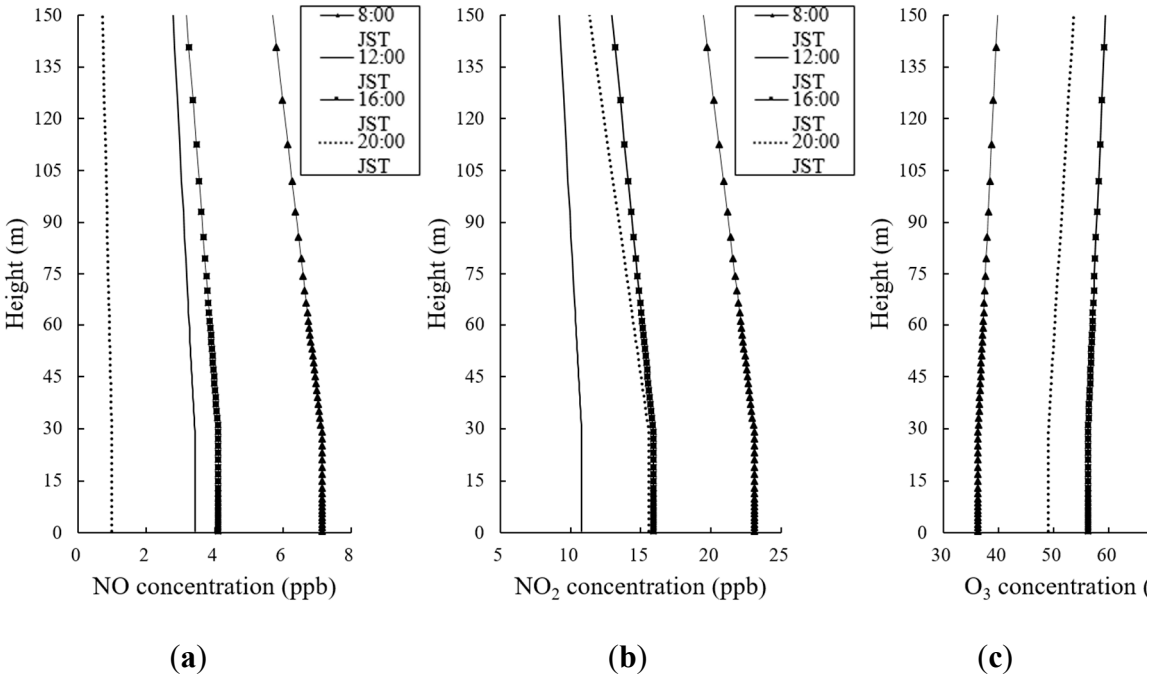

Figure S2. Boundary conditions for (**a**) NO, (**b**) NO_2, and (**c**) O_3 concentrations at 08:00, 12:00, 16:00, and 20:00 JST.

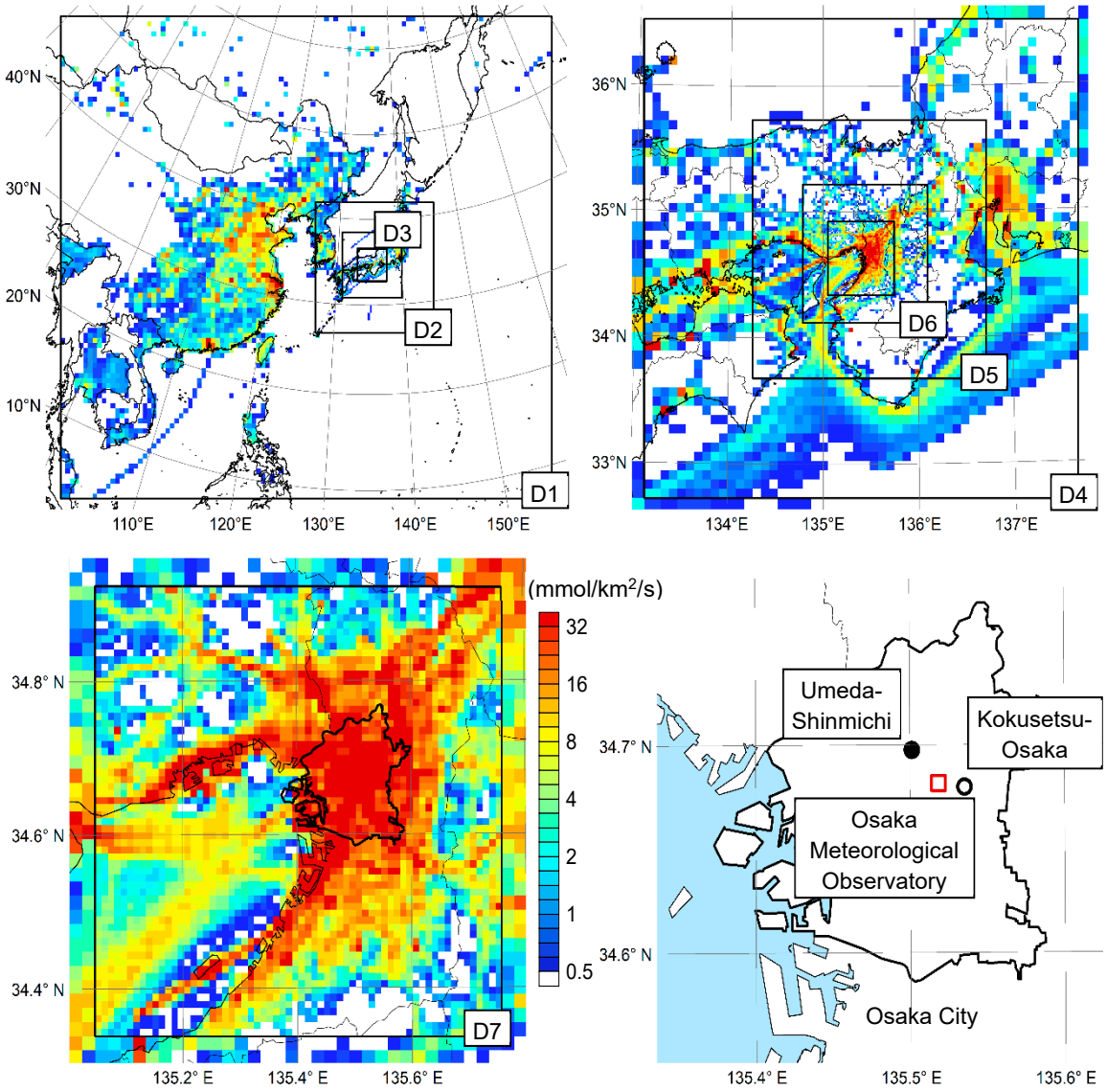

Figure S3. Spatial distributions of mean NO_x emission intensity in CMAQ modeling domains from D1 covering East Asia to D7 covering Osaka Prefecture, and locations of observation sites in Osaka City used for model validations.

Table S1. WRF and CMAQ configurations.

	Parameter	Setting
	Simulation period	24 June 24–31 August 2010
	Map projection	Lambert conformal conic
	Horizontal grid spacing	64 (D1), 32 (D2), 16 (D3), 8 (D4), 4 (D5), 2 (D6), 1 (D7) km
	Vertical domain	Surface to 100 hPa with 30 layers (middle height of 1st, 2nd, 3rd layer ≅ 28, 92, 190 m)
WRF v3.7	Horizontal grid number	120 × 108 (D1), 64 × 64 (D2), 64 × 64 (D3), 64 × 64 (D4), 68 × 68 (D5), 72 × 72 (D6), 76 × 76 (D7)
	Topography/Landuse	30″ data by United States Geological Survey (USGS) / 30″ data by USGS, 100-m data by Geospatial Information Authority of Japan
	Initial and boundary	Atmosphere over Japan: Mesoscale model grid point value data by JMA; Sea surface temperature: High-resolution, real-time, global sea surface temperature analysis data by U.S. National Centers for Environmental Prediction (NCEP); Others: Final operational global analysis data by NCEP
	Grid nudging	G_{uv} = 3.0 (D1), 3.0 (D2), 3.0 (D3), 2.4 (D4), 1.2 (D5), 0.6 (D6), 0.3 (D7) × 10^{-4} s^{-1} for the entire simulation period and vertical layers
	Microphysics	WRF single-moment 6-class scheme
	Cumulus	Kain-Fritsch scheme (D1, D2, D3)
	Planetary boundary layer	Yonsei University scheme
	Surface	Noah land surface model
	Long-/Short-wave radiation	Rapid radiative transfer model/Dudhia scheme
CMAQ v5.1	Horizontal grid number	108 × 96 (D1), 52 × 52 (D2), 52 × 52 (D3), 52 × 52 (D4), 56 × 56 (D5), 60 × 60 (D6), 64 × 64 (D7)
	Meteorology	Hourly WRF output data processed with Meteorology-Chemistry Interface Processor v4.3
	Initial and boundary	Model for Ozone and Related Chemical Tracers v4
	Emission	Anthropogenic in Japan: JEI-DB (vehicle), Emission inventory by Ocean Policy Research Foundation (ship), EAGrid2010-JAPAN (others); Anthropogenic outside Japan: Emission inventory for Hemispheric Transport of Air Pollution v2; Biogenic: Model of Emissions of Gases and Aerosols from Nature v2.04
	Gas phase chemistry	CB05
	Aerosol phase chemistry	Sixth generation CMAQ aerosol module

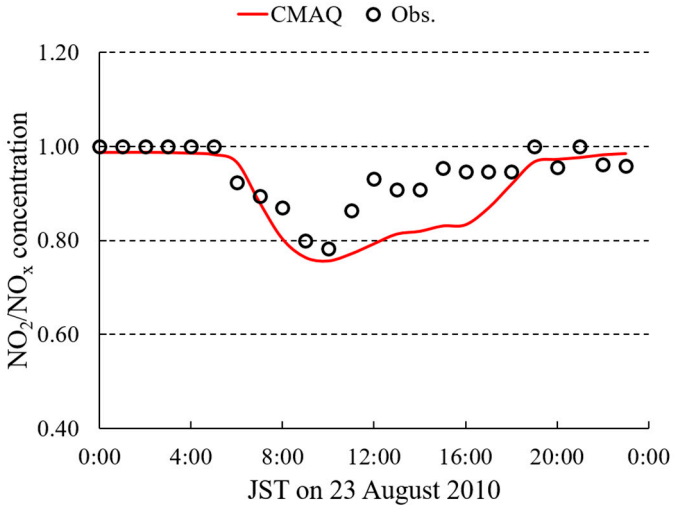

Figure S4. Diurnal variations of the CMAQ-simulated and observed NO_2/NO_x concentration ratio at the Kokusetsu-Osaka station for monitoring ambient air pollution on 23 August 2010.

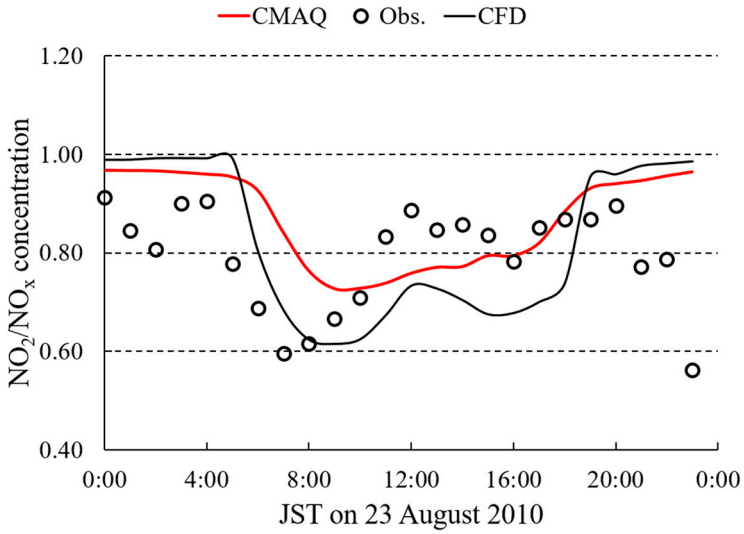

Figure S5. Diurnal variations of the CMAQ-simulated, observed and CFD-simulated NO_2/NO_x concentration ratio at the Umeda-Shinmichi station for monitoring roadside air pollution on 23 August 2010.

Figure S4 shows the diurnal variations of the CMAQ-simulated and observed NO_2/NO_x concentration ratio at the Kokusetsu-Osaka station for monitoring ambient air pollution on 23 August 2010. Figure S5 shows the diurnal variations of the CMAQ-simulated, observed and CFD-simulated NO_2/NO_x concentration ratio at the Umeda-Shinmichi station for monitoring roadside air pollution on 23 August 2010. In the morning hours, a sharp decrease of the NO_2/NO_x ratio is observed due to the increase of the NO_x emission rates related to the morning traffic (Figure 5). In the night hours, due to the NO_x titration an increase of the NO_2/NO_x ratio is observed. Figures S4 and S5 demonstrate the behavior of the reactive pollutants (NO, NO_2 and O_3) depending on the time of the day and the NO_x emission rates.

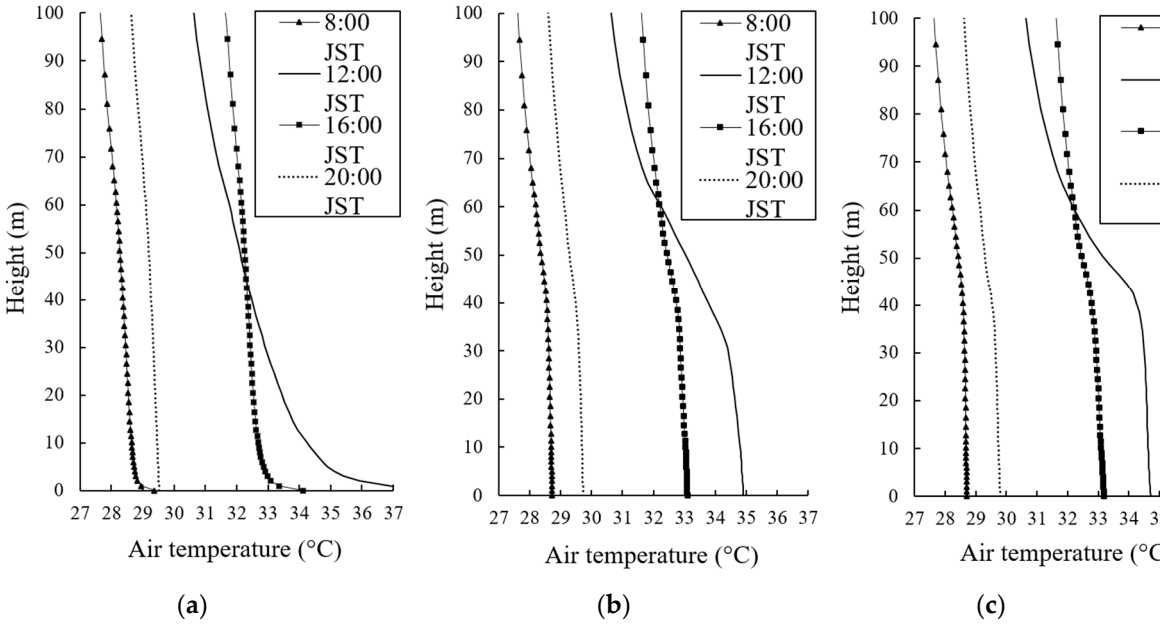

Figure S6. Vertical air temperature profiles at 08:00, 12:00, 16:00, and 20:00 JST on National Route 25 for the points (**a**) P_1 located at y = 230 m; (**b**) P_2 located at y = 350 m; (**c**) P_3 located at y = 390 m (Figure 2a).

Figure S6 shows the vertical air temperature profiles as a result of the surface energy model and the building envelope model at 08:00, 12:00, 16:00, and 20:00 JST for the reference points P_1 (y = 230 m), P_2 (y = 350 m), and P_3 (y = 390 m), located in the middle of National Route 25 as indicated in Figure 2a. The three locations showed higher temperatures at 12:00 JST and 16:00 JST. The high temperature on the road at 12:00 JST is because of the sun position overhead, and at 16:00 JST, because of the radiation already absorbed by buildings. In location P_1 (y = 230 m), the air temperature shows a different profile in comparison with P_2 and P_3 due to the free circulation of the wind in the southern part of the analysis area. At locations P_2 (y = 350 m) and P_3 (y = 390 m), the air temperature decreases when moving away from the surface level, especially when above the level of the building roof (~30 meters). At 12:00 JST, the slight westerly wind coming in the north of the urban canyon gives a reduction in the air temperature, but at the same time a wind flowing from south to east (Figure 3 and Figure 7) in the street canyon prevents the westerly wind from reaching further into the street canyon. At 16:00 JST, hot air is moved from the middle of the street canyon to northern areas, as a consequence, the air temperature at location P_3 (y = 390 m) is slightly higher than at location P_2 (y = 350 m).